Particulate nitrate photolysis as a possible driver of rising tropospheric ozone

Viral Shah[1,2]*, Christoph A. Keller[1,3], K. Emma Knowland[1,3], Amy Christiansen[4], Lu Hu[5], Haolin Wang[6], Xiao Lu[6], Becky Alexander[7], Daniel J. Jacob[8]

[1]Global Modeling and Assimilation Office (GMAO), NASA Goddard Space Flight Center, Greenbelt, MD 20770, USA.

[2]Science Systems and Applications, Inc., Lanham, MD 20706, USA.

[3]GESTAR II, Morgan State University, Baltimore, MD 21251, USA.

[4]Division of Energy, Matter & Systems, University of Missouri-Kansas City, Kansas City, MO 64108, USA.

[5]Department of Chemistry and Biochemistry, University of Montana, Missoula, MT 59812, USA.

[6]School of Atmospheric Sciences, Sun Yat-sen University, Zhuhai, Guangdong, 519082, P.R. China.

[7]Department of Atmospheric Sciences, University of Washington, Seattle, WA 98195, USA.

[8]Harvard John A. Paulson School of Engineering and Applied Sciences, Harvard University, Cambridge, MA 02138, USA.

Corresponding author: Viral Shah (viral.shah@nasa.gov)

Key Points:

- Particulate nitrate photolysis improves the consistency of tropospheric ozone in the GEOS-Chem model with observations
- Increase in particulate nitrate due to falling SO_2 and rising NH_3 emissions could augment the long-term increase in tropospheric ozone
- Better characterization of the mechanism and rates of particulate nitrate photolysis is needed

Abstract

Tropospheric ozone is an air pollutant and a greenhouse gas whose anthropogenic production is limited principally by the supply of nitrogen oxides (NO_x) from combustion. Tropospheric ozone in the northern hemisphere has been rising despite the flattening of NO_x emissions in recent decades. Here we propose that this sustained increase could result from the photolysis of nitrate particles (pNO_3^-) to regenerate NO_x. Including pNO_3^- photolysis in the GEOS-Chem atmospheric chemistry model improves the consistency with ozone observations. Our simulations show that pNO_3^- concentrations have increased since the 1960s because of rising ammonia and falling SO_2 emissions, augmenting the increase in ozone in the northern extratropics by about 50% to better match the observed ozone trend. pNO_3^- will likely continue to increase through 2050, which would drive a continued increase in ozone even as NO_x emissions decrease. More work is needed to better understand the mechanism and rates of pNO_3^- photolysis.

Plain Language Summary

In the troposphere, ozone is an air pollutant and a greenhouse gas. Tropospheric ozone forms from reactions involving carbon monoxide and volatile organic compounds in the presence of nitrogen oxides. Global emissions of nitrogen oxides have been leveling off in the past few decades, yet tropospheric ozone levels have kept on rising. We propose that this rise in ozone could be driven by a growing source of nitrogen oxides from the photolysis of nitrate particles, which have become more abundant due to falling sulfur dioxide and rising ammonia emissions. We find that including nitrate particle photolysis in an atmospheric chemistry model improves its consistency with the observed ozone distribution and trends. Our results point to the importance of considering nitrate particle photolysis for future projections of climate forcing from tropospheric ozone, and the need for further work to reduce the uncertainty in the mechanism and rates of the process.

1 Introduction

Tropospheric ozone is a short-lived climate forcer and a highly reactive gas that can damage human cells and tissue and reduce plant productivity. It forms from the oxidation of

carbon monoxide (CO), methane, and volatile organic compounds in the presence of nitrogen oxides ($NO_x \equiv NO+NO_2$). A smaller amount is transported from the stratosphere. Tropospheric ozone concentrations in the northern midlatitudes have risen by about 50% since the early 20th century because of rising anthropogenic emissions of ozone precursors (Tarasick et al., 2019). This trend has continued into the 21st century (Ziemke et al., 2019; Christiansen et al., 2022; Gaudel et al., 2020), although the rise in global precursor emissions has slowed down (Hoesly et al., 2018). Between the 1990s and 2017, ozone concentrations in the northern hemisphere increased by an average of 2 ppbv per decade in the free troposphere, the layer between ~2 km and the tropopause (Christiansen et al., 2022; Gaudel et al., 2020). Ozone increases in the free troposphere have a larger effect on climate than increases near the surface (Lacis et al., 1990). Free tropospheric ozone also contributes to ozone pollution at the surface (Lin et al., 2017; Colombi et al., 2023). However, global atmospheric chemistry models cannot account for the observed ozone increase (Christiansen et al., 2022; Gaudel et al., 2020; Skeie et al., 2020; H. Wang et al., 2022), implying that key processes are missing. It is important to identify these processes to improve our ability to make accurate future projections of climate forcing and air pollution from tropospheric ozone.

Intercomparisons of global atmospheric chemistry models show major differences in their computed global production and loss of tropospheric ozone (Stevenson et al., 2006; Wu et al., 2007; Hu et al., 2017; Young et al., 2018). Only a few models include tropospheric halogen chemistry, an important sink for ozone and NO_x (Saiz-Lopez et al., 2012; Sherwen et al., 2016; X. Wang et al., 2021). When included in the widely used GEOS-Chem model, halogen chemistry lowers the tropospheric ozone burden by 15% (X. Wang et al., 2021). At the same time, many models including GEOS-Chem underestimate ozone production over the tropical oceans because of an underestimate in NO_x concentrations (Travis et al., 2020; Hao Guo et al., 2023). The combination of halogen chemistry and low tropical NO_x has led recent versions of GEOS-Chem to underestimate global tropospheric ozone (X. Wang et al., 2021).

The photolysis of nitrate particles (pNO_3^-) has been proposed as a major route for recycling NO_x over the oceans (Ye et al., 2016; Reed et al., 2017; Kasibhatla et al., 2018; Andersen et al., 2023). pNO_3^- is produced by the gas-particle partitioning of nitric acid (HNO_3), the dominant sink of NO_x, at low temperature, high humidity, and low aerosol acidity, which is

associated with high ammonia, low sulfate, and freshly emitted sea salt aerosols. Photolysis of nitrate ions in aqueous solutions produces nitrous acid (HONO) and NO_2, which volatilize to the gas phase (Mack & Bolton, 1999):

$$NO_3^- + h\nu \xrightarrow{H_2O\ (l)} HONO(g) + OH^- + O(^3P) \quad \text{(R1a)}$$

$$\xrightarrow{H_2O\ (l)} NO_2(g) + OH^- + OH \quad \text{(R1b)}$$

Using aircraft-based HONO observations over the oceans, studies have inferred a pNO_3^- photolysis frequency on the order of 10^{-4} s^{-1} (Ye et al., 2016; Andersen et al., 2023), which is about two orders of magnitude faster than the photolysis frequency of gas-phase HNO_3 or nitrate in bulk solutions, likely because of enhancement of nitrate at the aerosol surface (Ye et al., 2017; Andersen et al., 2023). These fast rates are supported by laboratory studies on ambient pNO_3^- (Bao et al., 2018; Gen et al., 2019; Ye et al., 2017). Shah et al. (2023) showed that including pNO_3^- photolysis in GEOS-Chem corrects the NO_x underestimate over the oceans and increases the production of tropospheric ozone in the model. However, some field and laboratory studies suggest that the reaction is too slow ($<10^{-5}$ s^{-1}) to be a significant path for recycling NO_x (Romer et al., 2018; Shi et al., 2021; Y. Zhu et al., 2022).

Here we show that including the parameterization of pNO_3^- photolysis from Shah et al. (2023) improves the ability of the GEOS-Chem model to simulate the observed tropospheric ozone distribution as well as the trends in the northern midlatitudes since the mid-1990s. Further simulations indicate that increasing pNO_3^- concentrations has augmented the growth in the tropospheric ozone burden since the middle of the 20th century and could continue to do so until the middle of the 21st century.

2 Materials and Methods

2.1 Ozone measurements

We use observations of ozone vertical profiles from the global ozonesonde network (Tarasick et al., 2021; Stauffer et al., 2022), and the In-service Aircraft for a Global Observing System (IAGOS) program (Petzold et al., 2015). We use ozonesonde data from the following archives: Harmonization and Evaluation of Ground-based Instruments for Free Tropospheric Ozone Measurements group (HEGIFTOM v2), NOAA Earth System Research Laboratory -

Global Monitoring Division (Sterling et al., 2018), the Southern Hemisphere ADditional OZonesondes (SHADOZ; Thompson et al., 2017; Witte et al., 2017, 2018), and the World Ozone and Ultraviolet Data Center (WOUDC; WOUDC Ozone Monitoring Community et al., 2015). Ozonesondes measure ozone using an electrochemical cell with accuracy of better than ±10% (Tarasick et al., 2019; Thompson et al., 2019). The ozonesonde launch frequency varies among sites from once a month to thrice a week. We exclude stations with less than 2 profiles in a month and less than 8 months of observations, and aggregate the observations at each site to monthly means. The ozonesonde stations used in this work are listed in Supporting Information S1.

The IAGOS program provides ozone observations using commercial passenger aircraft (Petzold et al., 2015). In this work, we only use the vertical profile observations from the take-off and landing portions of the flights, excluding observations from the cruise portion. The IAGOS measurements are made using a dual-beam ultraviolet absorption photometer, with an accuracy of ±2 ppbv (Nédélec et al., 2015; Blot et al., 2021). We aggregate the profiles into 8 areas to account for the irregular sampling frequency at any one airport, excluding areas with less than 2 profiles in a month and less than 8 months of observations (Supporting Information S1). We further aggregate the observations in each area to monthly means. Comparisons of the two datasets show the IAGOS measurements to be low relative to the ozonesonde measurements by 5–8% (Staufer et al., 2014; Tarasick et al., 2019).

2.2 GEOS-Chem

We simulate tropospheric ozone using the GEOS-Chem atmospheric chemistry model (version 14.2.0; doi: 10.5281/zenodo.8411433) driven by meteorology from the NASA Global Modeling and Assimilation Office's (GMAO) Modern-Era Retrospective analysis for Research and Applications, Version 2 (MERRA-2) reanalysis (Gelaro et al., 2017). GEOS-Chem includes a detailed representation of tropospheric and stratospheric gas and aerosol chemistry (Eastham et al., 2014; Gao et al., 2022; Sherwen et al., 2016; Travis et al., 2016), with recent updates to the tropospheric halogen chemistry (X. Wang et al., 2021). Sea salt aerosol debromination was previously disabled in recent applications of the model, despite evidence that it takes place (Sander et al., 2003), because it caused excessive ozone depletion in the marine boundary layer (Shah et al., 2023). This was partly due to an error in how the titration of sea salt aerosol

alkalinity was represented in the model. This error is now fixed, and we include sea salt aerosol debromination in our simulation. We also reduce the loss of ozone by iodine radicals by including the uptake of HOI, IONO, and $IONO_2$ on alkaline sea salt aerosols as I^-, and by limiting the hydrolysis of $IONO_2$ to acidic aerosols. Ozone dry deposition in the model was recently updated to explicitly consider the reaction of ozone with sea surface I^- (Pound et al., 2020), and to use a higher surface resistance over snow and ice (Barten et al., 2021).

pNO_3^- photolysis in GEOS-Chem follows the original implementation of Kasibhatla et al. (2018) with modifications from Shah et al. (2023). The photolysis frequency of pNO_3^- is calculated by scaling the photolysis frequency of HNO_3 by an enhancement factor (EF). The EF is taken to be 100 for coarse mode pNO_3^- and between 10 and 100 for fine mode pNO_3^- depending on the fraction of pNO_3^- in sea salt aerosols (Shah et al., 2023):

$$\mathrm{EF} = \max\left(10, 100 \times \frac{1}{1+\frac{[\mathrm{pNO_3^-}]}{[\mathrm{SSA}]}}\right) \quad (1)$$

Here, $[\mathrm{pNO_3^-}]$ and [SSA] are the molar concentrations in air of fine mode pNO_3^- and sea salt aerosol. The molar concentration of sea salt is taken as $[\mathrm{SSA}] = 2.39\,[\mathrm{Na^+}]$ based on the fraction of Na^+ in seawater (Millero et al., 2008), and where Na^+ is the chemically inert sea salt aerosol species simulated by GEOS-Chem. The HONO:NO_2 yield is taken to be 2:1 (Kasibhatla et al., 2018). The thermodynamic partitioning of HNO_3 to fine mode pNO_3^- is computed with ISORROPIA II (Fountoukis & Nenes, 2007; Pye et al., 2009). Coarse mode pNO_3^- forms by the uptake of HNO_3 on sea salt aerosols (X. Wang et al., 2019). Uptake of HNO_3 on dust is not included here, though it is an option in GEOS-Chem (Fairlie et al., 2010). Photolysis frequencies in the model are calculated using Fast-JX (Bian & Prather, 2002; Eastham et al., 2014). As described in Shah et al. (2023), equation (1) fits the current ensemble of laboratory and field evidence for pNO_3^- photolysis, and it corrects previous GEOS-Chem low bias in simulating NO_x concentrations over the remote oceans.

Our main simulation is conducted for 2018 (with a spin-up period of six months) at a 4° latitude ×5° longitude resolution. For comparison with the ozonesonde and IAGOS measurements, we sample the model at the measurement location and within a 3-hour window of the measurement time. To evaluate the long-term changes in tropospheric ozone, we conduct additional simulations for the years 1960, 1980, 1995, and 2050 using year-specific

anthropogenic emissions and methane concentrations but constant (2018) meteorology and natural emissions. For each simulation we conduct a parallel simulation without pNO_3^- photolysis. Details about emission inventories and the tropospheric ozone budget in GEOS-Chem are in the Supporting Information S1.

3 Results and discussion

3.1 Tropospheric ozone distribution in 2018

Figure 1 shows the annual mean ozone distribution in the middle troposphere (800–400 hPa or ~2–7 km altitude) from the ozonesonde and IAGOS observations and GEOS-Chem simulations in 2018. Figure 2 shows the observed and simulated ozone vertical profiles between the surface and 200 hPa, and the seasonal variation of mid-tropospheric ozone concentrations over six regions. The global mean ozone concentration in the middle troposphere in the ensemble of ozonesonde and IAGOS observations is 47.4 ppbv. This is reproduced by GEOS-Chem with a mean bias of 2.8 ppbv, and within the observational uncertainty of ~8% implied by the bias between the ozonesonde and IAGOS measurements. The simulated ozone vertical profiles and seasonal variations also align with the observations in most regions (Fig. 2). The model overestimates ozone observations in the tropics, which could be from an overestimate in lightning NO_x emissions. The global lightning NO_x emission in GEOS-Chem is 6 Tg N a^{-1}, but there is large uncertainty in this source with estimates ranging from 2 to 8 Tg N a^{-1} (Schumann & Huntrieser, 2007).

The ozone concentrations from a simulation without pNO_3^- photolysis are on average 2–6 ppbv lower than those in the base simulation, but they are still largely consistent with the observations within their uncertainty (Fig. 2). An exception is the northern extratropics in spring, where the effect of pNO_3^- photolysis is strongest, and excluding it introduces a negative bias of up to 10 ppbv compared to the observations over the Arctic, North America and Europe, and East Asia (bottom panel of Fig. 2). pNO_3^- concentrations are highest in spring because of efficient lifting to the free troposphere combined with relatively low temperatures and seasonally rising emissions of ammonia from agricultural sources. Actinic flux is also relatively high in spring to enable pNO_3^- photolysis as well as ozone production. A low ozone bias in spring in the absence of pNO_3^- photolysis had been previously reported in recent versions of GEOS-Chem and

attributed to halogen chemistry (Christiansen et al., 2022; H. Wang et al., 2022; X. Wang et al., 2021; L. Zhu et al., 2019). This bias is remedied by including pNO_3^- photolysis in the model, as also found by Colombi et al. (2023) and Yang et al. (2023) in comparison with ozonesonde and aircraft observations over South Korea in May–June 2016.

3.2 Multi-decadal trends in tropospheric ozone

Ozone concentrations in the free troposphere have increased by 1–6 ppbv decade^{-1} in the northern hemisphere since the mid-1990s (Christiansen et al., 2022; Gaudel et al., 2020; H. Wang et al., 2022), but previous versions of GEOS-Chem could not capture that trend (Christiansen et al., 2022; H. Wang et al., 2022). pNO_3^- concentrations in the northern midlatitudes have most likely increased over this period because of decreasing aerosol acidity due to decreasing sulfate and increasing ammonia (Bauer et al., 2020; Paulot et al., 2018). Here, we examine the effect of rising pNO_3^- concentrations on ozone trends by conducting simulations for the year 1995. We switch only the anthropogenic emissions and methane levels to 1995 values, keeping the meteorology, and natural emissions constant. There is no long-term trend in global lightning NO_x emissions (Kaplan & Lau, 2022). Wang et al. (2022) found that climatic factors contribute little to the global ozone trend between 1995 and 2018.

Figure 3 compares the 1995 to 2018 change in mid-tropospheric ozone concentrations in the base GEOS-Chem simulation and the simulation without pNO_3^- photolysis to the observed trends in the ozonesonde and IAGOS data calculated by Christiansen et al. (2022) and Wang et al. (2022). Both simulations and the observations show the fastest increase in tropospheric ozone over Asia, reflecting the increase in ozone precursor emissions in the region over this period (Hoesly et al., 2018; Kurokawa & Ohara, 2020). However, the ozone increase in the base simulation is larger than that in the simulation without pNO_3^- photolysis, particularly in the northern midlatitudes, and more consistent with the observed trends. Over East Asia, the ozonesonde and IAGOS observations show mid-tropospheric ozone trends of 2.1–3.3 ppbv decade^{-1}. In comparison, the base GEOS-Chem simulation shows an increase of 2.3–2.7 ppbv decade^{-1}, but the simulation without pNO_3^- photolysis shows an increase of 1.4–1.9 ppbv decade^{-1}, suggesting that about a third of the increase in ozone over East Asia since the mid-1990s is driven by increasing pNO_3^-. The base simulation also reproduces the trend in the IAGOS data

over North America better than the simulation without pNO_3^- photolysis, but it overestimates the IAGOS trend over Europe. The trends in the ozonesonde data over North America and Europe vary substantially, which suggests that they are strongly affected by meteorological variability (Christiansen et al., 2022).

pNO_3^- concentrations in the northern midlatitudes in the model double between 1995 and 2018, mainly because of falling SO_2 emissions and rising ammonia emissions. According to the Community Emissions Data System (CEDS) inventory (Hoesly et al., 2018) used in our simulations, global anthropogenic SO_2 emissions over this period fell by 55% due to better emission controls in power plants, while anthropogenic ammonia emissions rose by 20% due to increased agricultural activity. pNO_3^- formation in the northern midlatitude free troposphere is limited by high aerosol acidity (Nault et al., 2021). Aerosol acidity drops when there is less sulfate and more ammonia, allowing more HNO_3 to condense as pNO_3^- (Hongyu Guo et al., 2016). The increase in pNO_3^- in the model happens mostly in the free troposphere, where NO_x concentrations are sensitive to pNO_3^- photolysis (Dang et al., 2023). At the surface, pNO_3^- concentrations decrease over US and Europe, consistent with the observed trends (Hand et al., 2020; Ciarelli et al., 2019), but increase over Asia. Free tropospheric pNO_3^- also increases due to the 50% increase in global aircraft NO_x emissions between 1995 and 2018 (Simone et al., 2013).

Emissions of SO_2, ammonia, and NO_x have changed substantially since the middle of the 20th century and further changes are expected in the future (Gidden et al., 2019; Hoesly et al., 2018). We examined the effect of these changes on long-term trends of pNO_3^- and ozone by conducting additional simulations for the years 1960, 1980, and 2050. For 2050, we use the SSP2-4.5 emissions scenario from Phase 6 of the Coupled Model Intercomparison Project (CMIP6). SSP2-4.5 is a middle-of-the-road scenario in which future emissions largely follow the current trends (Fricko et al., 2017). Again, we only consider changes in anthropogenic emissions and methane concentrations.

Figure 4 shows the 1960–2050 change in the tropospheric ozone burden in the base GEOS-Chem simulation and the simulation without pNO_3^- photolysis. It also shows the simulated tropospheric burdens of sulfate, HNO_3, and pNO_3^-, and global emissions of SO_2, NO_x, and ammonia for 1960–2050. The ozone burden increases between 1960 and 2050 in both

simulations largely because of increase in methane, NO_x and CO emissions. However, the burden in the base simulation increases by 86 Tg in this period, compared to an increase of 67 Tg in the simulation without pNO_3^- photolysis, because of the increasing burden of pNO_3^-. The burden of pNO_3^- has increased much faster than the burden of HNO_3, reflecting the trends in SO_2 and ammonia emissions. Between 2018 and 2050, the base simulation projects an increase in the ozone burden by 12 Tg (under the SSP2-4.5 scenario), double the increase in the simulation without pNO_3^- photolysis, because of projected increase in pNO_3^-, despite a decrease in the HNO_3 burden and NO_x emissions. This result is not specific to the SSP2-4.5 scenario, as most SSP scenarios project a decrease in SO_2 and increase in ammonia emissions between now and 2050, making it likely that increasing pNO_3^- will continue to amplify the trend in tropospheric ozone.

4 Conclusions

Photolysis of nitrate particles (pNO_3^-) is generally not included in global atmospheric chemistry models but we show here that it improves the tropospheric ozone simulation in the GEOS-Chem model and can help account for the observed multi-decadal trends in ozone. pNO_3^- photolysis increases simulated free tropospheric ozone concentrations in the northern extratropics in the spring by up to 10 ppbv and counteracts the springtime ozone loss by halogen radicals that would otherwise cause a low bias in ozone in the model. We find that increasing pNO_3^- concentrations due to falling SO_2 and rising ammonia emissions globally since the 1980s have amplified the increase in the tropospheric ozone burden and explain over a third of the observed growth in free tropospheric ozone over the northern midlatitudes between 1995 and 2018. Increasing pNO_3^- will likely continue to raise the tropospheric ozone burden through 2050.

The significant effect of pNO_3^- photolysis on tropospheric ozone calls for further work to characterize its mechanism and rates. Rate estimates for this reaction are highly variable, with values ranging from 1 to 1000 times the HNO_3 photolysis frequency, but it is not fully clear what drives this variability (Andersen et al., 2023). Simulation of pNO_3^- also remains a challenge in models (Shah et al., 2018; Zhai et al., 2021) and is highly sensitive to the parameterization of wet deposition (Luo et al., 2020). Improvements in model representation of these processes would increase confidence in our assessment of the role of pNO_3^- photolysis as a driver of tropospheric ozone trends.

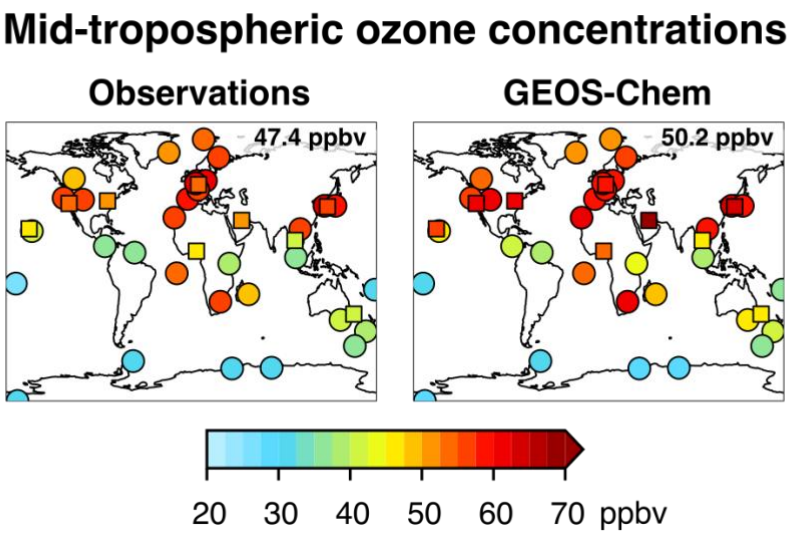

Figure 1. Annual mean ozone concentrations in the middle troposphere (800–400 hPa) in 2018. The left panel shows observed ozone concentrations from the ozonesonde (circles) and the IAGOS (squares) datasets. The right panel shows results from the GEOS-Chem simulation sampled at the measurement times and locations. The mean mid-tropospheric ozone concentrations from the observations and the model at the measurement sites are shown inset.

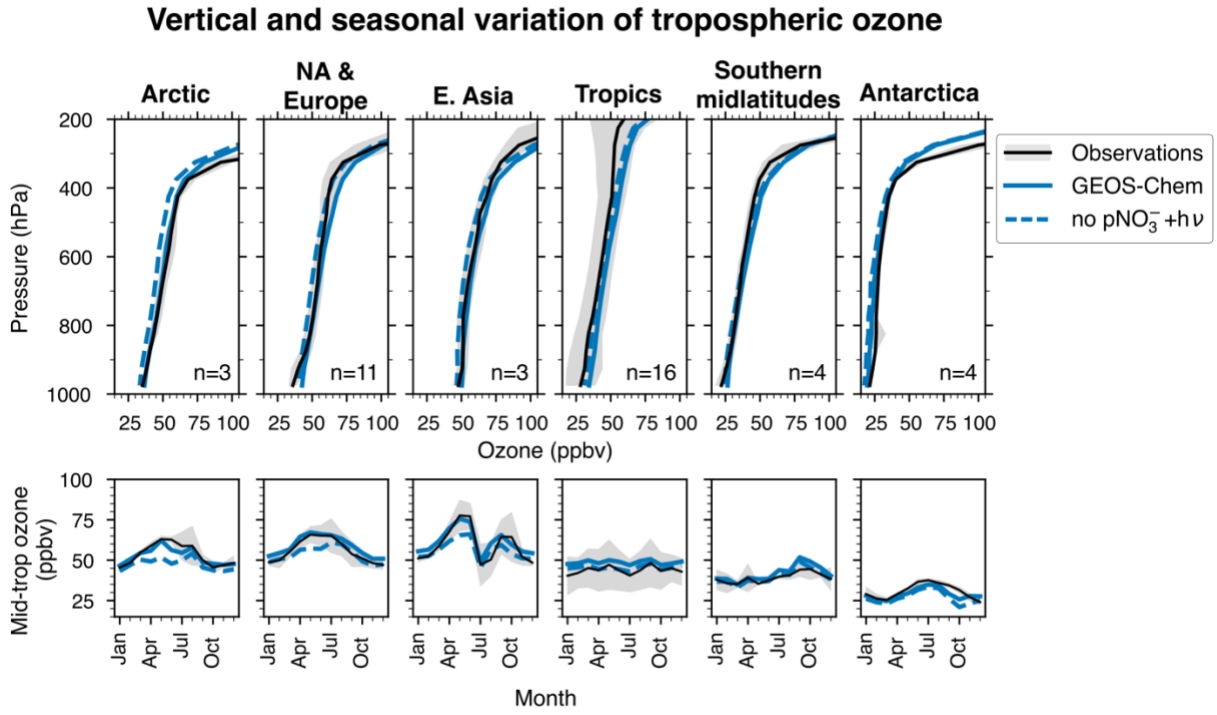

Figure 2. Vertical profiles and seasonal variations of tropospheric ozone over six regions in 2018. The top panels show the annual mean ozone concentrations between the surface and 200 hPa from the ozonesonde and IAGOS observations, and GEOS-Chem simulations aggregated into six regions. The bottom panels show the observed and simulated monthly mean ozone concentrations in the middle troposphere (800–400 hPa) over the six regions. The figure shows results from the base GEOS-Chem simulation (solid line) and from a simulation without pNO_3^- photolysis (dashed line). The number of sites (ozonesonde and IAGOS) in each region (n) is indicated in the top panels (Tables S1 and S2). The shaded areas denote ±1 standard deviation of the annual mean ozone profiles (top panel) and the monthly mid-tropospheric ozone concentrations (bottom panel) at the measurement sites in each region.

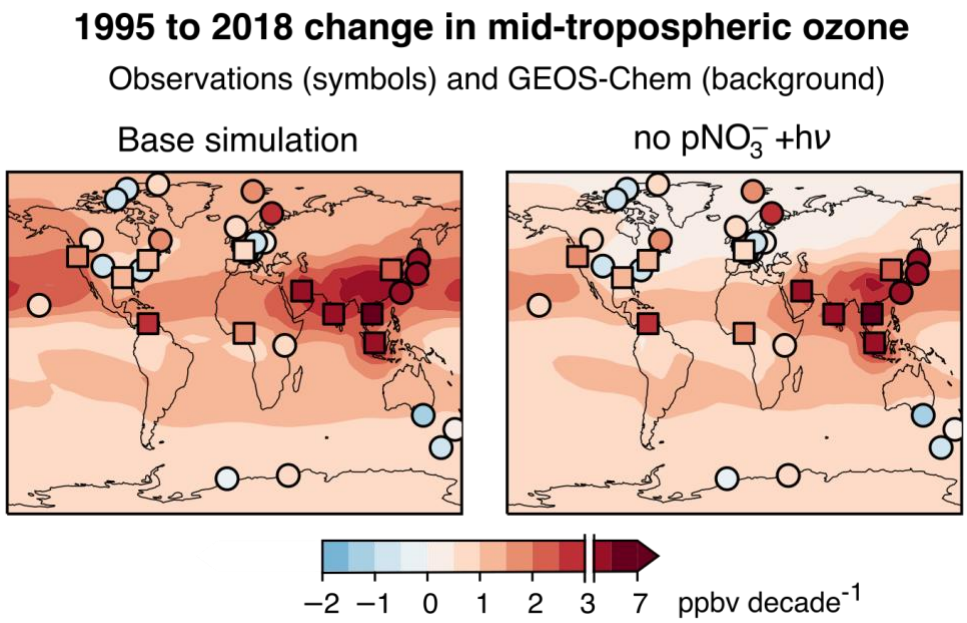

Figure 3. 1995 to 2018 change in ozone concentrations in the middle troposphere. The top panels show the change of 800–400 hPa ozone concentrations in response to the change in anthropogenic emissions between 1995 and 2018 in the GEOS-Chem base simulation and a simulation without pNO_3^- photolysis. Also shown are the trends in mid-tropospheric ozone from ozonesonde (circles) and IAGOS (squares) observations as reported by Christiansen et al. (2022) and Wang et al. (2022), respectively. These trends were reported for 25 ozonesonde sites for 1990–2017 (1980–2017 for nine sites), and in 11 IAGOS areas for 1995–2017.

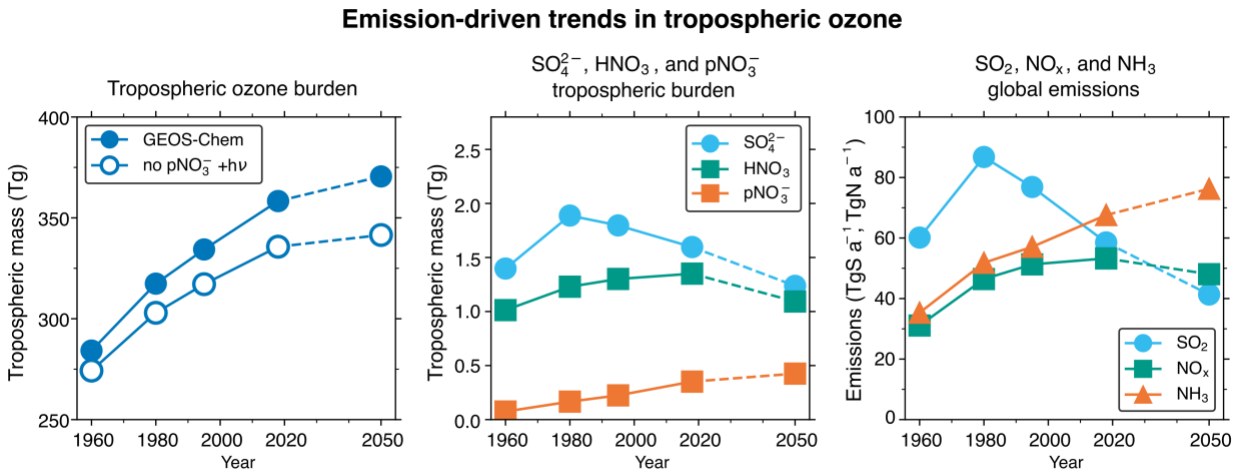

Figure 4. Emission-driven changes in tropospheric ozone burden, tropospheric burdens of sulfate, HNO_3, and pNO_3^-, and global emissions of SO_2, NO_x, and NH_3. The burdens are from the base GEOS-Chem simulations using time-varying anthropogenic emissions and methane concentrations (for years 1960, 1980, 1995, 2018, and 2050), but constant meteorology (year 2018). Historical anthropogenic emissions are from the Community Emissions Data System (Hoesly et al., 2018), and emissions for 2050 are from the SSP2-4.5 scenario (Gidden et al., 2019) used in Phase 6 of the Coupled Model Intercomparison Project (CMIP6). The left panel also shows tropospheric ozone burdens from the GEOS-Chem simulation without pNO_3^- photolysis. The right panel shows emissions from all sources in GEOS-Chem.

Acknowledgments

Work at the GMAO was supported by the NASA Satellite Needs Working Group (SNWG). Work at Harvard was supported by the Harvard–NUIST Joint Laboratory for Air Quality and Climate, the Samsung PM2.5 Strategic Research Program, and the US EPA Science to Achieve Results (STAR) program. A.C. and L.H. acknowledge additional support from NOAA (grants: NA19OAR4310174 and NA19OAR4310176). B.A. acknowledges funding from NSF (grant: AGS 2109323). We thank N. Colombi (Harvard), R.M. Stauffer, A.M. Thompson (NASA GSFC), M.J. Evans (University of York), and B.H. Henderson (US EPA) for helpful discussions. We are grateful to all contributors to the SHADOZ, NOAA GMD, WOUDC, HEGIFTOM and IAGOS datasets.

Open Research

The measurements and model used in this study are publicly available. Ozone observations are available at https://hegiftom.meteo.be (HEGIFTOM), ftp://ftp.cmdl.noaa.gov/ozww/Ozonesonde/ (NOAA), https://tropo.gsfc.nasa.gov/shadoz/ (SHADOZ), doi:10.14287/10000008 (WOUDC), and https://iagos.aeris-data.fr/ (IAGOS). The GEOS-Chem source code is available at doi:10.5281/zenodo.8411433.

References

Andersen, S. T., Carpenter, L. J., Reed, C., Lee, J. D., Chance, R., Sherwen, T., et al. (2023). Extensive field evidence for the release of HONO from the photolysis of nitrate aerosols. *Science Advances*, *9*(3), eadd6266. https://doi.org/10.1126/sciadv.add6266

Bao, F., Li, M., Zhang, Y., Chen, C., & Zhao, J. (2018). Photochemical Aging of Beijing Urban $PM_{2.5}$: HONO Production. *Environmental Science & Technology*, *52*(11), 6309–6316. https://doi.org/10.1021/acs.est.8b00538

Barten, J. G. M., Ganzeveld, L. N., Steeneveld, G.-J., & Krol, M. C. (2021). Role of oceanic ozone deposition in explaining temporal variability in surface ozone at High Arctic sites. *Atmospheric Chemistry and Physics*, *21*(13), 10229–10248. https://doi.org/10.5194/acp-21-10229-2021

Bauer, S. E., Tsigaridis, K., Faluvegi, G., Kelley, M., Lo, K. K., Miller, R. L., et al. (2020). Historical (1850–2014) Aerosol Evolution and Role on Climate Forcing Using the GISS ModelE2.1 Contribution to CMIP6. *Journal of Advances in Modeling Earth Systems*, *12*(8), e2019MS001978. https://doi.org/10.1029/2019MS001978

Bian, H., & Prather, M. J. (2002). Fast-J2: Accurate Simulation of Stratospheric Photolysis in Global Chemical Models. *Journal of Atmospheric Chemistry*, *41*(3), 281–296. https://doi.org/10.1023/A:1014980619462

Blot, R., Nedelec, P., Boulanger, D., Wolff, P., Sauvage, B., Cousin, J.-M., et al. (2021). Internal consistency of the IAGOS ozone and carbon monoxide measurements for the last 25 years. *Atmospheric Measurement Techniques*, *14*(5), 3935–3951. https://doi.org/10.5194/amt-14-3935-2021

Christiansen, A. E., Mickley, L. J., Liu, J., Oman, L. D., & Hu, L. (2022). Multidecadal increases in global tropospheric ozone derived from ozonesonde and surface site observations: can models reproduce ozone trends? *Atmospheric Chemistry and Physics*, *22*(22), 14751–14782. https://doi.org/10.5194/acp-22-14751-2022

Ciarelli, G., Theobald, M. R., Vivanco, M. G., Beekmann, M., Aas, W., Andersson, C., et al. (2019). Trends of inorganic and organic aerosols and precursor gases in Europe: insights from the EURODELTA multi-model experiment over the 1990–2010 period. *Geoscientific Model Development*, *12*(12), 4923–4954. https://doi.org/10.5194/gmd-12-4923-2019

Colombi, N. K., Jacob, D. J., Yang, L. H., Zhai, S., Shah, V., Grange, S. K., et al. (2023). Why is ozone in South Korea and the Seoul metropolitan area so high and increasing? *Atmospheric Chemistry and Physics*, *23*(7), 4031–4044. https://doi.org/10.5194/acp-23-4031-2023

Dang, R., Jacob, D. J., Shah, V., Eastham, S. D., Fritz, T. M., Mickley, L. J., et al. (2023). Background nitrogen dioxide (NO 2) over the United States and its implications for satellite observations and trends: effects of nitrate photolysis, aircraft, and open fires. *Atmospheric Chemistry and Physics*, *23*(11), 6271–6284. https://doi.org/10.5194/acp-23-6271-2023

Eastham, S. D., Weisenstein, D. K., & Barrett, S. R. H. (2014). Development and Evaluation of the Unified Tropospheric–Stratospheric Chemistry Extension (UCX) for the Global Chemistry-Transport Model GEOS-Chem. *Atmospheric Environment*, *89*, 52–63. https://doi.org/10.1016/j.atmosenv.2014.02.001

Fairlie, T. D., Jacob, D. J., Dibb, J. E., Alexander, B., Avery, M. A., van Donkelaar, A., & Zhang, L. (2010). Impact of mineral dust on nitrate, sulfate, and ozone in transpacific Asian pollution plumes. *Atmospheric Chemistry and Physics*, *10*(8), 3999–4012. https://doi.org/10.5194/acp-10-3999-2010

Fountoukis, C., & Nenes, A. (2007). ISORROPIA II: a computationally efficient thermodynamic equilibrium model for K^+–Ca^{2+}–Mg^{2+}–NH_4^+–Na^+–SO_4^{2-}–NO_3^-–Cl^-–H_2O aerosols. *Atmos. Chem. Phys.*, *7*(17), 4639–4659. https://doi.org/10.5194/acp-7-4639-2007

Fricko, O., Havlik, P., Rogelj, J., Klimont, Z., Gusti, M., Johnson, N., et al. (2017). The marker quantification of the Shared Socioeconomic Pathway 2: A middle-of-the-road scenario for the 21st century. *Global Environmental Change*, *42*, 251–267. https://doi.org/10.1016/j.gloenvcha.2016.06.004

Gao, C. Y., Heald, C. L., Katich, J. M., Luo, G., & Yu, F. (2022). Remote Aerosol Simulated During the Atmospheric Tomography (ATom) Campaign and Implications for Aerosol Lifetime. *Journal of Geophysical Research: Atmospheres*, *127*(22). https://doi.org/10.1029/2022JD036524

Gaudel, A., Cooper, O. R., Chang, K.-L., Bourgeois, I., Ziemke, J. R., Strode, S. A., et al. (2020). Aircraft observations since the 1990s reveal increases of tropospheric ozone at multiple locations across the Northern Hemisphere. *Science Advances*, *6*(34), eaba8272. https://doi.org/10.1126/sciadv.aba8272

Gelaro, R., McCarty, W., Suárez, M. J., Todling, R., Molod, A., Takacs, L., et al. (2017). The Modern-Era Retrospective Analysis for Research and Applications, Version 2 (MERRA-2). *Journal of Climate*, *30*(14), 5419–5454. https://doi.org/10.1175/JCLI-D-16-0758.1

Gen, M., Zhang, R., Huang, D. D., Li, Y., & Chan, C. K. (2019). Heterogeneous Oxidation of SO_2 in Sulfate Production during Nitrate Photolysis at 300 nm: Effect of pH, Relative Humidity, Irradiation Intensity, and the Presence of Organic Compounds. *Environmental Science & Technology*, *53*(15), 8757–8766. https://doi.org/10.1021/acs.est.9b01623

Gidden, M. J., Riahi, K., Smith, S. J., Fujimori, S., Luderer, G., Kriegler, E., et al. (2019). Global emissions pathways under different socioeconomic scenarios for use in CMIP6: a dataset of harmonized emissions trajectories through the end of the century. *Geoscientific Model Development*, *12*(4), 1443–1475. https://doi.org/10.5194/gmd-12-1443-2019

Guo, Hao, Flynn, C. M., Prather, M. J., Strode, S. A., Steenrod, S. D., Emmons, L., et al. (2023). Heterogeneity and chemical reactivity of the remote troposphere defined by aircraft measurements – corrected. *Atmospheric Chemistry and Physics*, *23*(1), 99–117. https://doi.org/10.5194/acp-23-99-2023

Guo, Hongyu, Sullivan, A. P., Campuzano-Jost, P., Schroder, J. C., Lopez-Hilfiker, F. D., Dibb, J. E., et al. (2016). Fine particle pH and the partitioning of nitric acid during winter in the northeastern United States. *Journal of Geophysical Research: Atmospheres*, *121*(17), 10,355-10,376. https://doi.org/10.1002/2016JD025311

Hand, J. L., Prenni, A. J., Copeland, S., Schichtel, B. A., & Malm, W. C. (2020). Thirty years of the Clean Air Act Amendments: Impacts on haze in remote regions of the United States (1990–2018). *Atmospheric Environment*, *243*, 117865. https://doi.org/10.1016/j.atmosenv.2020.117865

Hoesly, R. M., Smith, S. J., Feng, L., Klimont, Z., Janssens-Maenhout, G., Pitkanen, T., et al. (2018). Historical (1750–2014) anthropogenic emissions of reactive gases and aerosols from the Community Emissions Data System (CEDS). *Geosci. Model Dev.*, *11*(1), 369–408. https://doi.org/10.5194/gmd-11-369-2018

Hu, L., Jacob, D. J., Liu, X., Zhang, Y., Zhang, L., Kim, P. S., et al. (2017). Global budget of tropospheric ozone: Evaluating recent model advances with satellite (OMI), aircraft (IAGOS), and ozonesonde observations. *Atmospheric Environment*, *167*, 323–334. https://doi.org/10.1016/j.atmosenv.2017.08.036

Kaplan, J. O., & Lau, K. H.-K. (2022). World Wide Lightning Location Network (WWLLN) Global Lightning Climatology (WGLC) and time series, 2022 update. *Earth System Science Data*, *14*(12), 5665–5670. https://doi.org/10.5194/essd-14-5665-2022

Kasibhatla, P., Sherwen, T., Evans, M. J., Carpenter, L. J., Reed, C., Alexander, B., et al. (2018). Global impact of nitrate photolysis in sea-salt aerosol on NO_x, OH, and O_3; in the marine boundary layer. *Atmospheric Chemistry and Physics*, *18*(15), 11185–11203. https://doi.org/10.5194/acp-18-11185-2018

Kurokawa, J., & Ohara, T. (2020). Long-term historical trends in air pollutant emissions in Asia: Regional Emission inventory in ASia (REAS) version 3. *Atmospheric Chemistry and Physics*, *20*(21), 12761–12793. https://doi.org/10.5194/acp-20-12761-2020

Lacis, A. A., Wuebbles, D. J., & Logan, J. A. (1990). Radiative forcing of climate by changes in the vertical distribution of ozone. *Journal of Geophysical Research: Atmospheres*, *95*(D7), 9971–9981. https://doi.org/10.1029/JD095iD07p09971

Lin, M., Horowitz, L. W., Payton, R., Fiore, A. M., & Tonnesen, G. (2017). US surface ozone trends and extremes from 1980 to 2014: quantifying the roles of rising Asian emissions, domestic controls, wildfires, and climate. *Atmospheric Chemistry and Physics*, *17*(4), 2943–2970. https://doi.org/10.5194/acp-17-2943-2017

Luo, G., Yu, F., & Moch, J. M. (2020). Further improvement of wet process treatments in GEOS-Chem v12.6.0: impact on global distributions of aerosols and aerosol precursors. *Geoscientific Model Development*, *13*(6), 2879–2903. https://doi.org/10.5194/gmd-13-2879-2020

Mack, J., & Bolton, J. R. (1999). Photochemistry of nitrite and nitrate in aqueous solution: a review. *Journal of Photochemistry and Photobiology A: Chemistry*, *128*(1–3), 1–13. https://doi.org/10.1016/S1010-6030(99)00155-0

Millero, F. J., Feistel, R., Wright, D. G., & McDougall, T. J. (2008). The composition of Standard Seawater and the definition of the Reference-Composition Salinity Scale. *Deep Sea Research Part I: Oceanographic Research Papers*, *55*(1), 50–72. https://doi.org/10.1016/j.dsr.2007.10.001

Nault, B. A., Campuzano-Jost, P., Day, D. A., Jo, D. S., Schroder, J. C., Allen, H. M., et al. (2021). Chemical transport models often underestimate inorganic aerosol acidity in remote regions of the atmosphere. *Communications Earth & Environment*, *2*(1), 93. https://doi.org/10.1038/s43247-021-00164-0

Nédélec, P., Blot, R., Boulanger, D., Athier, G., Cousin, J.-M., Gautron, B., et al. (2015). Instrumentation on commercial aircraft for monitoring the atmospheric composition on a global scale: the IAGOS system, technical overview of ozone and carbon monoxide measurements. *Tellus B: Chemical and Physical Meteorology*, *67*(1), 27791. https://doi.org/10.3402/tellusb.v67.27791

Paulot, F., Paynter, D., Ginoux, P., Naik, V., & Horowitz, L. W. (2018). Changes in the aerosol direct radiative forcing from 2001 to 2015: observational constraints and regional mechanisms. *Atmospheric Chemistry and Physics*, *18*(17), 13265–13281. https://doi.org/10.5194/acp-18-13265-2018

Petzold, A., Thouret, V., Gerbig, C., Zahn, A., Brenninkmeijer, C. A. M., Gallagher, M., et al. (2015). Global-scale atmosphere monitoring by in-service aircraft – current achievements and future prospects of the European Research Infrastructure IAGOS. *Tellus B: Chemical and Physical Meteorology*, *67*(1), 28452. https://doi.org/10.3402/tellusb.v67.28452

Pound, R. J., Sherwen, T., Helmig, D., Carpenter, L. J., & Evans, M. J. (2020). Influences of oceanic ozone deposition on tropospheric photochemistry. *Atmospheric Chemistry and Physics*, *20*(7), 4227–4239. https://doi.org/10.5194/acp-20-4227-2020

Pye, H. O. T., Liao, H., Wu, S., Mickley, L. J., Jacob, D. J., Henze, D. K., & Seinfeld, J. H. (2009). Effect of changes in climate and emissions on future sulfate-nitrate-ammonium aerosol levels in the United States. *Journal of Geophysical Research*, *114*(D1). https://doi.org/10.1029/2008JD010701

Reed, C., Evans, M. J., Crilley, L. R., Bloss, W. J., Sherwen, T., Read, K. A., et al. (2017). Evidence for renoxification in the tropical marine boundary layer. *Atmospheric Chemistry and Physics*, *17*(6), 4081–4092. https://doi.org/10.5194/acp-17-4081-2017

Romer, P. S., Wooldridge, P. J., Crounse, J. D., Kim, M. J., Wennberg, P. O., Dibb, J. E., et al. (2018). Constraints on Aerosol Nitrate Photolysis as a Potential Source of HONO and NO_x. *Environmental Science & Technology*, *52*(23), 13738–13746. https://doi.org/10.1021/acs.est.8b03861

Saiz-Lopez, A., Lamarque, J.-F., Kinnison, D. E., Tilmes, S., Ordóñez, C., Orlando, J. J., et al. (2012). Estimating the climate significance of halogen-driven ozone loss in the tropical marine troposphere. *Atmospheric Chemistry and Physics*, *12*(9), 3939–3949. https://doi.org/10.5194/acp-12-3939-2012

Sander, R., Keene, W. C., Pszenny, A. A. P., Arimoto, R., Ayers, G. P., Baboukas, E., et al. (2003). Inorganic bromine in the marine boundary layer: a critical review. *Atmospheric Chemistry and Physics*, *3*(5), 1301–1336. https://doi.org/10.5194/acp-3-1301-2003

Schumann, U., & Huntrieser, H. (2007). The global lightning-induced nitrogen oxides source. *Atmospheric Chemistry and Physics*, *7*(14), 3823–3907. https://doi.org/10.5194/acp-7-3823-2007

Shah, V., Jaeglé, L., Thornton, J. A., Lopez-Hilfiker, F. D., Lee, B. H., Schroder, J. C., et al. (2018). Chemical feedbacks weaken the wintertime response of particulate sulfate and nitrate to emissions reductions over the eastern United States. *Proceedings of the National Academy of Sciences*, *115*(32), 8110. https://doi.org/10.1073/pnas.1803295115

Shah, V., Jacob, D. J., Dang, R., Lamsal, L. N., Strode, S. A., Steenrod, S. D., et al. (2023). Nitrogen oxides in the free troposphere: implications for tropospheric oxidants and the interpretation of satellite NO_2 measurements. *Atmospheric Chemistry and Physics*, *23*(2), 1227–1257. https://doi.org/10.5194/acp-23-1227-2023

Sherwen, T., Schmidt, J. A., Evans, M. J., Carpenter, L. J., Gro\s smann, K., Eastham, S. D., et al. (2016). Global impacts of tropospheric halogens (Cl, Br, I) on oxidants and composition in GEOS-Chem. *Atmospheric Chemistry and Physics*, *16*(18), 12239–12271. https://doi.org/10.5194/acp-16-12239-2016

Shi, Q., Tao, Y., Krechmer, J. E., Heald, C. L., Murphy, J. G., Kroll, J. H., & Ye, Q. (2021). Laboratory Investigation of Renoxification from the Photolysis of Inorganic Particulate Nitrate. *Environmental Science & Technology*, *55*(2), 854–861. https://doi.org/10.1021/acs.est.0c06049

Simone, N. W., Stettler, M. E. J., & Barrett, S. R. H. (2013). Rapid estimation of global civil aviation emissions with uncertainty quantification. *Transportation Research Part D: Transport and Environment*, *25*, 33–41. https://doi.org/10.1016/j.trd.2013.07.001

Skeie, R. B., Myhre, G., Hodnebrog, Ø., Cameron-Smith, P. J., Deushi, M., Hegglin, M. I., et al. (2020). Historical total ozone radiative forcing derived from CMIP6 simulations. *Npj Climate and Atmospheric Science*, *3*(1), 32. https://doi.org/10.1038/s41612-020-00131-0

Staufer, J., Staehelin, J., Stübi, R., Peter, T., Tummon, F., & Thouret, V. (2014). Trajectory matching of ozonesondes and MOZAIC measurements in the UTLS – Part 2: Application to the global ozonesonde network. *Atmospheric Measurement Techniques*, *7*(1), 241–266. https://doi.org/10.5194/amt-7-241-2014

Stauffer, R. M., Thompson, A. M., Kollonige, D. E., Tarasick, D. W., Van Malderen, R., Smit, H. G. J., et al. (2022). An Examination of the Recent Stability of Ozonesonde Global Network Data. *Earth and Space Science*, *9*(10), e2022EA002459. https://doi.org/10.1029/2022EA002459

Sterling, C. W., Johnson, B. J., Oltmans, S. J., Smit, H. G. J., Jordan, A. F., Cullis, P. D., et al. (2018). Homogenizing and estimating the uncertainty in NOAA's long-term vertical ozone profile records

measured with the electrochemical concentration cell ozonesonde. *Atmospheric Measurement Techniques*, *11*(6), 3661–3687. https://doi.org/10.5194/amt-11-3661-2018

Stevenson, D. S., Dentener, F. J., Schultz, M. G., Ellingsen, K., Van Noije, T. P. C., Wild, O., et al. (2006). Multimodel ensemble simulations of present-day and near-future tropospheric ozone. *Journal of Geophysical Research*, *111*(D8), D08301. https://doi.org/10.1029/2005JD006338

Tarasick, D. W., Galbally, I. E., Cooper, O. R., Schultz, M. G., Ancellet, G., Leblanc, T., et al. (2019). Tropospheric Ozone Assessment Report: Tropospheric ozone from 1877 to 2016, observed levels, trends and uncertainties. *Elementa: Science of the Anthropocene*, *7*, 39. https://doi.org/10.1525/elementa.376

Tarasick, D. W., Smit, H. G. J., Thompson, A. M., Morris, G. A., Witte, J. C., Davies, J., et al. (2021). Improving ECC Ozonesonde Data Quality: Assessment of Current Methods and Outstanding Issues. *Earth and Space Science*, *8*(3). https://doi.org/10.1029/2019EA000914

Thompson, A. M., Witte, J. C., Sterling, C., Jordan, A., Johnson, B. J., Oltmans, S. J., et al. (2017). First Reprocessing of Southern Hemisphere Additional Ozonesondes (SHADOZ) Ozone Profiles (1998–2016): 2. Comparisons With Satellites and Ground-Based Instruments. *Journal of Geophysical Research: Atmospheres*, *122*(23). https://doi.org/10.1002/2017JD027406

Thompson, A. M., Smit, H. G. J., Witte, J. C., Stauffer, R. M., Johnson, B. J., Morris, G., et al. (2019). Ozonesonde Quality Assurance: The JOSIE–SHADOZ (2017) Experience. *Bulletin of the American Meteorological Society*, *100*(1), 155–171. https://doi.org/10.1175/BAMS-D-17-0311.1

Travis, K. R., Jacob, D. J., Fisher, J. A., Kim, P. S., Marais, E. A., Zhu, L., et al. (2016). Why do models overestimate surface ozone in the Southeast United States? *Atmospheric Chemistry and Physics*, *16*(21), 13561–13577. https://doi.org/10.5194/acp-16-13561-2016

Travis, K. R., Heald, C. L., Allen, H. M., Apel, E. C., Arnold, S. R., Blake, D. R., et al. (2020). Constraining remote oxidation capacity with ATom observations. *Atmospheric Chemistry and Physics*, *20*(13), 7753–7781. https://doi.org/10.5194/acp-20-7753-2020

Wang, H., Lu, X., Jacob, D. J., Cooper, O. R., Chang, K.-L., Li, K., et al. (2022). Global tropospheric ozone trends, attributions, and radiative impacts in 1995–2017: an integrated analysis using aircraft (IAGOS) observations, ozonesonde, and multi-decadal chemical model simulations. *Atmospheric Chemistry and Physics*, *22*(20), 13753–13782. https://doi.org/10.5194/acp-22-13753-2022

Wang, X., Jacob, D. J., Eastham, S. D., Sulprizio, M. P., Zhu, L., Chen, Q., et al. (2019). The role of chlorine in global tropospheric chemistry. *Atmospheric Chemistry and Physics*, *19*(6), 3981–4003. https://doi.org/10.5194/acp-19-3981-2019

Wang, X., Jacob, D. J., Downs, W., Zhai, S., Zhu, L., Shah, V., et al. (2021). Global tropospheric halogen (Cl, Br, I) chemistry and its impact on oxidants. *Atmospheric Chemistry and Physics*, *21*(18), 13973–13996. https://doi.org/10.5194/acp-21-13973-2021

Witte, J. C., Thompson, A. M., Smit, H. G. J., Fujiwara, M., Posny, F., Coetzee, G. J. R., et al. (2017). First reprocessing of Southern Hemisphere ADditional OZonesondes (SHADOZ) profile records (1998–2015): 1. Methodology and evaluation. *Journal of Geophysical Research: Atmospheres*, *122*(12), 6611–6636. https://doi.org/10.1002/2016JD026403

Witte, J. C., Thompson, A. M., Smit, H. G. J., Vömel, H., Posny, F., & Stübi, R. (2018). First Reprocessing of Southern Hemisphere ADditional OZonesondes Profile Records: 3. Uncertainty in Ozone Profile and Total Column. *Journal of Geophysical Research: Atmospheres*, *123*(6), 3243–3268. https://doi.org/10.1002/2017JD027791

WOUDC Ozone Monitoring Community, World Meteorological Organization-Global Atmosphere Watch Program (WMO-GAW), & World Ozone And Ultraviolet Radiation Data Centre (WOUDC). (2015). Ozone [Http://woudc.org/about/formats.php]. https://doi.org/10.14287/10000001

Wu, S., Mickley, L. J., Jacob, D. J., Logan, J. A., Yantosca, R. M., & Rind, D. (2007). Why are there large differences between models in global budgets of tropospheric ozone? *Journal of Geophysical Research*, *112*(D5). https://doi.org/10.1029/2006JD007801

Yang, L. H., Jacob, D. J., Colombi, N. K., Zhai, S., Bates, K. H., Shah, V., et al. (2023). Tropospheric NO_2 vertical profiles over South Korea and their relation to oxidant chemistry: implications for geostationary satellite retrievals and the observation of NO_2 diurnal variation from space. *Atmospheric Chemistry and Physics*, *23*(4), 2465–2481. https://doi.org/10.5194/acp-23-2465-2023

Ye, C., Zhou, X., Pu, D., Stutz, J., Festa, J., Spolaor, M., et al. (2016). Rapid cycling of reactive nitrogen in the marine boundary layer. *Nature*, *532*(7600), 489–491. https://doi.org/10.1038/nature17195

Ye, C., Zhang, N., Gao, H., & Zhou, X. (2017). Photolysis of Particulate Nitrate as a Source of HONO and NO_x. *Environmental Science & Technology*, *51*(12), 6849–6856. https://doi.org/10.1021/acs.est.7b00387

Young, P. J., Naik, V., Fiore, A. M., Gaudel, A., Guo, J., Lin, M. Y., et al. (2018). Tropospheric Ozone Assessment Report: Assessment of global-scale model performance for global and regional ozone distributions, variability, and trends. *Elementa: Science of the Anthropocene*, *6*, 10. https://doi.org/10.1525/elementa.265

Zhai, S., Jacob, D. J., Brewer, J. F., Li, K., Moch, J. M., Kim, J., et al. (2021). Relating geostationary satellite measurements of aerosol optical depth (AOD) over East Asia to fine particulate matter (PM_{2.5}): insights from the KORUS-AQ aircraft campaign and GEOS-Chem model simulations. *Atmospheric Chemistry and Physics*, *21*(22), 16775–16791. https://doi.org/10.5194/acp-21-16775-2021

Zhu, L., Jacob, D. J., Eastham, S. D., Sulprizio, M. P., Wang, X., Sherwen, T., et al. (2019). Effect of Sea Salt Aerosol on Tropospheric Bromine Chemistry. *Atmospheric Chemistry and Physics*, *19*(9), 6497–6507. https://doi.org/10.5194/acp-19-6497-2019

Zhu, Y., Wang, Y., Zhou, X., Elshorbany, Y. F., Ye, C., Hayden, M., & Peters, A. J. (2022). An investigation into the chemistry of HONO in the marine boundary layer at Tudor Hill Marine Atmospheric Observatory in Bermuda. *Atmospheric Chemistry and Physics*, *22*(9), 6327–6346. https://doi.org/10.5194/acp-22-6327-2022

Ziemke, J. R., Oman, L. D., Strode, S. A., Douglass, A. R., Olsen, M. A., McPeters, R. D., et al. (2019). Trends in global tropospheric ozone inferred from a composite record of TOMS/OMI/MLS/OMPS satellite measurements and the MERRA-2 GMI simulation. *Atmospheric Chemistry and Physics*, *19*(5), 3257–3269. https://doi.org/10.5194/acp-19-3257-2019

Geophysical Research Letters

Supporting Information for

Particulate nitrate photolysis as a possible driver of rising tropospheric ozone

Viral Shah[1,2]*, Christoph A. Keller[1,3], K. Emma Knowland[1,3], Amy Christiansen[4], Lu Hu[5], Haolin Wang[6], Xiao Lu[6], Becky Alexander[7], Daniel J. Jacob[8]

[1]Global Modeling and Assimilation Office (GMAO), NASA Goddard Space Flight Center, Greenbelt, MD 20770, USA.
[2]Science Systems and Applications, Inc., Lanham, MD 20706, USA.
[3]GESTAR II, Morgan State University, Baltimore, MD 21251, USA.
[4]Division of Energy, Matter & Systems, University of Missouri-Kansas City, Kansas City, MO 64108, USA.
[5]Department of Chemistry and Biochemistry, University of Montana, Missoula, MT 59812, USA.
[6]School of Atmospheric Sciences, Sun Yat-sen University, Zhuhai, Guangdong, 519082, P.R. China.
[7]Department of Atmospheric Sciences, University of Washington, Seattle, WA 98195, USA.
[8]Harvard John A. Paulson School of Engineering and Applied Sciences, Harvard University, Cambridge, MA 02138, USA.

Contents of this file

Introduction

The following supporting information lists the ozonesonde sites (Table S1) and the In-service Aircraft for a Global Observing System (IAGOS) regions (Table S2) used in the study and provides additional details about the GEOS-Chem simulations (Text S1 and Tables S3, S4).

Text S1. Additional GEOS-Chem details

Ozone precursor emissions: Emissions in GEOS-Chem are calculated by the Harmonized Emissions Component (HEMCO, version 3.0; Keller et al., 2014; Lin et al., 2021) and include anthropogenic emissions from the Community Emissions Data System (CEDS, April '21 release, doi:10.5281/zenodo.4074245); Hoesly et al., 2018; McDuffie et al., 2020), aircraft emissions from the Aviation Emissions Inventory Code (AEIC, v2.0; Simone et al., 2013), fire emissions from the Global Fire Emissions Database (GFED4; Giglio et al., 2013), biogenic emissions using Model of Emissions of Gases and Aerosols from Nature (MEGAN, v2.1; Guenther et al., 2012), and nitrogen oxides (NO_x) emissions from lightning (Murray et al., 2012) and soils (Hudman et al., 2012). Table S3 lists the global NO_x, carbon monoxide (CO), and non-methane volatile organic compound emissions in our 2018 simulation. Methane concentrations are prescribed as surface boundary conditions based on the NOAA Global Monitoring Laboratory's flask measurements (Murray, 2016).

Our main simulations are for the year 2018, with additional simulations for 1960, 1980, 1995, and 2050 using year-specific anthropogenic emissions and methane concentrations. Historical emissions are from CEDS, and future emissions correspond to the CMIP6 SSP2-4.5 scenario. The CMIP6 emissions were implemented in HEMCO by Murray et al. (2021). The AEIC inventory provides historical aircraft emissions from 1990 to 2019. For 1960 and 1980, we scale down the AEIC emissions based on the change in the aircraft emissions in the CEDS inventory with respect to 1990. Aircraft emissions for 2050 are from the CMIP6 SSP2-4.5 scenario. The NOAA measurements of surface methane concentrations are available for 1979–present. For 1960, we use the CMIP6 historical methane concentrations (Meinshausen et al., 2017) and for 2050, projected methane concentrations for the SSP2-4.5 scenario (Meinshausen et al., 2020).

Tropospheric ozone budget in GEOS-Chem: Table S4 shows the global tropospheric ozone budget in GEOS-Chem in 2018. It is represented in terms of the odd oxygen family (O_x; $O_x \equiv O_3+NO_2+\ldots$, see table for full definition) to account for rapid cycling among these species. Ozone constitutes 99% of tropospheric O_x. The tropospheric O_x burden in GEOS-Chem for 2018 is 361 Tg, slightly higher than the range of 324–345 Tg inferred from ozonesonde and satellite measurements for 2010–16 (Gaudel et al., 2018), but within the range of models evaluated in the Tropospheric Ozone Assessment Report (TOAR) (Young et al., 2018) and CMIP6 (Griffiths et al., 2021). Particulate nitrate (pNO_3^-) photolysis increases the O_x burden by 7%, because of a 12% increase in chemical production of O_x to 5470 Tg a^{-1} on account of higher NO_x concentrations (Shah et al., 2023). The increase in O_x production in the model occurs largely over the oceans, where pNO_3^- photolysis has the largest effect on NO_x concentrations and the O_x production efficiency per unit NO_x is high.

The lifetime of O_x against chemical loss and deposition in our base simulation is 21.4 days (Table S4), which is lower than the TOAR and CMIP6 multi-model means. The models in these intercomparisons generally do not consider tropospheric halogen chemistry, which reduces O_x lifetime in GEOS-Chem by about 2 days (Wang et al., 2021). Many of the models also do not include pNO_3^- formation. Including pNO_3^- photolysis in GEOS-Chem decreases the O_x lifetime by 0.6 days, mostly because it increases tropospheric OH concentrations (Shah et al., 2023). pNO_3^- photolysis is also a direct sink of O_x through its HONO channel.

Table S1. Ozonesonde stations used for the evaluation of the 2018 simulations

Station	Latitude	Longitude	# of profiles[a]	Dataset[b]	Region
Ny-Ålesund	78.92°N	11.93°E	71	HEGIFTOM	Arctic
Scoresbysund	70.48°N	21.97°W	52	HEGIFTOM	Arctic
Sodankyla	67.37°N	26.65°E	25	HEGIFTOM	Arctic
Edmonton	53.54°N	114.1°W	35	HEGIFTOM	N. America
Lindenberg	52.21°N	14.12°E	62	WOUDC	Europe
De Bilt	52.1°N	5.18°E	54	HEGIFTOM	Europe
Uccle	50.8°N	4.35°E	142	HEGIFTOM	Europe
Payerne	46.49°N	6.57°E	133	WOUDC	Europe
Trinidad Head	40.8°N	124.2°W	49	NOAA	N. America
Madrid	40.47°N	3.68°W	51	HEGIFTOM	Europe
Boulder	40°N	105.3°W	50	NOAA	N. America
Tateno	36.06°N	140.1°E	46	WOUDC	E. Asia
Pohang	36.03°N	129.4°E	47	WOUDC	E. Asia
Izaña	28.3°N	16.48°W	35	HEGIFTOM	Tropics
Hanoi	21.01°N	105.8°E	30	SHADOZ	Tropics
Hilo	19.43°N	155.0°W	51	SHADOZ	Tropics
Costa Rica	9.94°N	84.04°W	34	SHADOZ	Tropics
Paramaribo	5.8°N	55.21°W	47	HEGIFTOM	Tropics
Kuala Lumpur	2.73°N	101.3°E	20	SHADOZ	Tropics
Nairobi	1.27°S	36.8°E	39	SHADOZ	Tropics
Ascension	7.58°S	14.24°W	43	SHADOZ	Tropics
Samoa	14.23°S	170.6°W	47	SHADOZ	Tropics
Fiji	18.13°S	178.4°E	41	SHADOZ	Tropics
Reunion	21.06°S	55.48°E	38	SHADOZ	Tropics
Irene	25.9°S	28.22°E	18	SHADOZ	Tropics
Broadmeadows	37.69°S	145.0 °E	48	WOUDC	Southern midlatitudes
Lauder	45°S	169.7°E	43	HEGIFTOM	Southern midlatitudes
Macquarie	54.5°S	159.0°E	51	WOUDC	Southern midlatitudes
Marambio	64.24°S	56.62°W	45	WOUDC	Antarctica
Davis	68.58°S	77.97°E	51	WOUDC	Antarctica
Syowa	69°S	39.58°E	51	WOUDC	Antarctica
South Pole	90°S	169°W	49	NOAA	Antarctica

a. Number of profiles in 2018.

b. HEGIFTOM: Harmonization and Evaluation of Ground-based Instruments for Free Tropospheric Ozone Measurements group; NOAA: NOAA Earth System Research Laboratory - Global Monitoring Division; SHADOZ: Southern Hemisphere ADditional Ozonesondes; WOUDC: World Ozone and Ultraviolet Data Center.

Table S2. IAGOS sites used for the evaluation of the 2018 simulations

Site	Latitude[a]	Longitude[a]	# of profiles[b]	Region
Western Europe	44–53°N	1°W – 14°E	312	Europe
Western US	32–48°N	105–123°W	207	N. America
Eastern US	28–45°N	71–97°W	53	N. America
China/Korea/Japan	26–43°N	113–142°E	232	E. Asia
Middle East	21–31°N	31–56°E	78	Tropics
Hawaii	19–22°N	156–158°W	279	Tropics
Central Africa	8°S–16°N	16°W–36°E	144	Tropics
Thailand	13.7°N	100.7°E	31	Tropics
Australia/New Zealand	27–43°S	144–175°E	46	Southern midlatitudes

a. Latitudinal and longitudinal range of the profiles aggregated at each site.

b. Number of profiles in 2018.

Table S3. Global NO_x, CO, and non-methane volatile organic compounds (VOC) emissions for 2018

Source	NO_x (TgN a^{-1})	CO (Tg a^{-1})	Non-methane VOC (Tg C a^{-1})
Fuel combustion[a]	33.8	534	104
Aircraft[b]	1.1	1.2	0.1
Fires[c]	5.7	315	23.7
Biogenic[d]	4.5	–	601[e]
Lightning[f]	6.3	–	–
Total	51.4	850	729

a. From the Community Emissions Data System (CEDS, April '21 release; Hoesly et al., 2018; McDuffie et al., 2020), except for ethane (Tzompa-Sosa et al., 2017) and propane (Xiao et al., 2008)

b. From the AEIC v2.0 inventory (Simone et al., 2013)

c. From GFEDv4.1s (Giglio et al., 2013)

d. VOC emissions include terrestrial plant emissions from MEGAN v2.1 (Guenther et al., 2012), emissions from plant decay (Millet et al., 2010), and oceanic sources (Fisher et al., 2018; Millet et al., 2010). Soil NO_x emissions are from (Hudman et al., 2012).

e. Includes 302 Tg of isoprene emissions.

f. From Murray et al. (2012).

Table S4. Global tropospheric ozone budget in GEOS-Chem and from model intercomparisons[a]

Model(s)	Burden (Tg)	Sources (Tg a^{-1})		Sinks (Tg a^{-1})		Lifetime (d)
		Chemical production	Strat-trop exchange[b]	Chemical loss	Deposition	
GEOS-Chem	361	5470	700	5070	1100[c]	21.4
No pNO_3^- photolysis[d]	338	4890	710	4580	1020[c]	22.0
TOAR[e]	340 ± 34	4937 ± 656	535 ± 161	4442 ± 570	996 ± 203	22.8[f]
CMIP6[g]	356 ± 31	4708 ± 589	277 ± 201	4122 ± 399	863 ± 40	25.5 ± 2.2

a. The budget is from the 2018 GEOS-Chem simulation and for the odd oxygen family ($O_x \equiv O_3 + NO_2 + HNO_3 + pNO_3^- + 2NO_3 + 3N_2O_5 + HNO_4$ + organic nitrates + $O(^1D) + XO + HOX + XNO_2 + 2XNO_3 + 2Cl_2O_2 + 2OClO + 2I_2O_2 + 2OIO + 3I_2O_3 + 4I_2O_4$; X ≡ Cl, Br, I). The troposphere is defined as extending from the surface to model layer just below the one that contains the monthly mean thermal tropopause diagnosed form the GMAO MERRA-2 data.
b. Stratosphere-troposphere exchange, inferred as the difference between the total sinks and chemical production as the net change in ozone mass during the one-year simulation is negligible.
c. Deposition includes dry and wet deposition. Wet deposition is mainly as HNO_3.
d. GEOS-Chem simulation without pNO_3^- photolysis
e. From Young et al. (2018). Values are for the year 2000. The intercomparison includes 49 models for the burden and about 33 models for the fluxes.
f. Calculated from the multimodel mean of the burden and sinks.
g. From Griffiths et al. (2021) and summarized in Szopa et al. (2021). Values are for the period 2005-14.

References

Fisher, J. A., Atlas, E. L., Barletta, B., Meinardi, S., Blake, D. R., Thompson, C. R., et al. (2018). Methyl, Ethyl, and Propyl Nitrates: Global Distribution and Impacts on Reactive Nitrogen in Remote Marine Environments. J. Geophys. Res. Atmos., 123(21), 12,429-12,451. https://doi.org/10.1029/2018JD029046

Gaudel, A., Cooper, O. R., Ancellet, G., Barret, B., Boynard, A., Burrows, J. P., et al. (2018). Tropospheric Ozone Assessment Report: Present-day distribution and trends of tropospheric ozone relevant to climate and global atmospheric chemistry model evaluation. Elementa: Science of the Anthropocene, 6, 39. https://doi.org/10.1525/elementa.291

Giglio, L., Randerson, J. T., & van der Werf, G. R. (2013). Analysis of daily, monthly, and annual burned area using the fourth-generation global fire emissions database (GFED4). J. Geophys. Res. Biogeo., 118(1), 317–328. https://doi.org/10.1002/jgrg.20042

Griffiths, P. D., Griffiths, P. T., Murray, L. T., Zeng, G., Archibald, A. T., Abraham, N. L., et al. (2021). Tropospheric ozone in CMIP6 simulations. Atmospheric Chemistry and Physics, 21(5), 4187–4218. https://doi.org/10.5194/acp-2019-1216

Guenther, A. B., Jiang, X., Heald, C. L., Sakulyanontvittaya, T., Duhl, T., Emmons, L. K., & Wang, X. (2012). The Model of Emissions of Gases and Aerosols from Nature version 2.1 (MEGAN2.1): an extended and updated framework for modeling biogenic emissions. Geoscientific Model Development, 5(6), 1471–1492. https://doi.org/10.5194/gmd-5-1471-2012

Hoesly, R. M., Smith, S. J., Feng, L., Klimont, Z., Janssens-Maenhout, G., Pitkanen, T., et al. (2018). Historical (1750–2014) anthropogenic emissions of reactive gases and aerosols from the Community Emissions Data System (CEDS). Geosci. Model Dev., 11(1), 369–408. https://doi.org/10.5194/gmd-11-369-2018

Hudman, R. C., Moore, N. E., Mebust, A. K., Martin, R. V., Russell, A. R., Valin, L. C., & Cohen, R. C. (2012). Steps towards a mechanistic model of global soil nitric oxide emissions: implementation and space based-constraints. Atmos. Chem. Phys., 12(16), 7779–7795. https://doi.org/10.5194/acp-12-7779-2012

Keller, C. A., Long, M. S., Yantosca, R. M., Da Silva, A. M., Pawson, S., & Jacob, D. J. (2014). HEMCO v1.0: a versatile, ESMF-compliant component for calculating emissions in atmospheric models. Geosci. Model Dev., 7(4), 1409–1417. https://doi.org/10.5194/gmd-7-1409-2014

Lin, H., Jacob, D. J., Lundgren, E. W., Sulprizio, M. P., Keller, C. A., Fritz, T. M., et al. (2021). Harmonized Emissions Component (HEMCO) 3.0 as a versatile emissions component for atmospheric models: application in the GEOS-Chem, NASA GEOS, WRF-GC, CESM2, NOAA GEFS-Aerosol, and NOAA UFS models. Geoscientific Model Development, 14(9), 5487–5506. https://doi.org/10.5194/gmd-14-5487-2021

McDuffie, E. E., Smith, S. J., O'Rourke, P., Tibrewal, K., Venkataraman, C., Marais, E. A., et al. (2020). A global anthropogenic emission inventory of atmospheric pollutants from sector- and fuel-specific sources (1970–2017): an application of the Community Emissions Data System (CEDS). Earth System Science Data, 12(4), 3413–3442. https://doi.org/10.5194/essd-12-3413-2020

Meinshausen, M., Vogel, E., Nauels, A., Lorbacher, K., Meinshausen, N., Etheridge, D. M., et al. (2017). Historical greenhouse gas concentrations for climate modelling (CMIP6). Geoscientific Model Development, 10(5), 2057–2116. https://doi.org/10.5194/gmd-10-2057-2017

Meinshausen, M., Nicholls, Z. R. J., Lewis, J., Gidden, M. J., Vogel, E., Freund, M., et al. (2020). The shared socio-economic pathway (SSP) greenhouse gas concentrations and their extensions to 2500. Geoscientific Model Development, 13(8), 3571–3605. https://doi.org/10.5194/gmd-13-3571-2020

Millet, D. B., Guenther, A., Siegel, D. A., Nelson, N. B., Singh, H. B., De Gouw, J. A., et al. (2010). Global atmospheric budget of acetaldehyde: 3-D model analysis and constraints from in-situ and satellite observations. Atmospheric Chemistry and Physics, 10(7), 3405–3425. https://doi.org/10.5194/acp-10-3405-2010

Murray, L. T. (2016). Lightning NO x and Impacts on Air Quality. Current Pollution Reports, 2(2), 115–133. https://doi.org/10.1007/s40726-016-0031-7

Murray, L. T., Jacob, D. J., Logan, J. A., Hudman, R. C., & Koshak, W. J. (2012). Optimized regional and interannual variability of lightning in a global chemical transport model constrained by LIS/OTD satellite data. Journal of Geophysical Research: Atmospheres, 117(D20). https://doi.org/10.1029/2012JD017934

Murray, L. T., Leibensperger, E. M., Orbe, C., Mickley, L. J., & Sulprizio, M. (2021). GCAP 2.0: a global 3-D chemical-transport model framework for past, present, and future climate scenarios. Geoscientific Model Development, 14(9), 5789–5823. https://doi.org/10.5194/gmd-14-5789-2021

Shah, V., Jacob, D. J., Dang, R., Lamsal, L. N., Strode, S. A., Steenrod, S. D., et al. (2023). Nitrogen oxides in the free troposphere: implications for tropospheric oxidants and the interpretation of satellite NO_2 measurements. Atmospheric Chemistry and Physics, 23(2), 1227–1257. https://doi.org/10.5194/acp-23-1227-2023

Simone, N. W., Stettler, M. E. J., & Barrett, S. R. H. (2013). Rapid estimation of global civil aviation emissions with uncertainty quantification. Transportation Research Part D: Transport and Environment, 25, 33–41. https://doi.org/10.1016/j.trd.2013.07.001

Szopa, S., Naik, V., Adhikary, B., Artaxo, P., Bernsten, T., Collins, W. D., et al. (2021). Short-Lived Climate Forcers. In Climate Change 2021: The Physical Science Basis. Contribution of Working Group I to the Sixth Assessment Report of the Intergovernmental Panel on Climate Change [Masson-Delmotte, V., P. Zhai, A. Pirani, S.L. Connors, C. Péan, S. Berger, N. Caud, Y. Chen, L. Goldfarb, M.I. Gomis, M. Huang, K. Leitzell, E. Lonnoy, J.B.R. Matthews, T.K. Maycock, T. Waterfield, O. Yelekçi, R. Yu, and B. Zhou (eds.)] (pp. 817–922). Cambridge, United Kingdom and New York, NY, USA: Cambridge University Press. https://doi.org/10.1017/9781009157896

Tzompa-Sosa, Z. A., Mahieu, E., Franco, B., Keller, C. A., Turner, A. J., Helmig, D., et al. (2017). Revisiting global fossil fuel and biofuel emissions of ethane. Journal of Geophysical Research: Atmospheres, 122(4), 2493–2512. https://doi.org/10.1002/2016JD025767

Wang, X., Jacob, D. J., Downs, W., Zhai, S., Zhu, L., Shah, V., et al. (2021). Global tropospheric halogen (Cl, Br, I) chemistry and its impact on oxidants. Atmospheric Chemistry and Physics, 21(18), 13973–13996. https://doi.org/10.5194/acp-21-13973-2021

Xiao, Y., Logan, J. A., Jacob, D. J., Hudman, R. C., Yantosca, R., & Blake, D. R. (2008). Global budget of ethane and regional constraints on U.S. sources. Journal of Geophysical Research, 113(D21), D21306. https://doi.org/10.1029/2007JD009415

Young, P. J., Naik, V., Fiore, A. M., Gaudel, A., Guo, J., Lin, M. Y., et al. (2018). Tropospheric Ozone Assessment Report: Assessment of global-scale model performance for global and regional ozone distributions, variability, and trends. Elementa: Science of the Anthropocene, 6, 10. https://doi.org/10.1525/elementa.265